INFRARED IMAGING OF M CAS B USING RAPID IMAGE MOTION COMPENSATION[1]

D. MCCARTHY, JR., T. HANCOCK, J. FREEMAN, B. MCLEOD, M. LLOYD-HART, AND D. COLUCCI
Steward Observatory, The University of Arizona, Tucson, Arizona 85721

P. WIZINOWICH
Keck Observatory Project,

M. CLAMPIN, D. GOLIMOWSKI, AND S. DURRANCE
Johns Hopkins University,

Received 19 May 1992; revised 14 September 1992

ABSTRACT

The orbital parameters and component masses of the μ Cas binary system can provide a measure of the helium abundance in the early Galaxy. In a continuing effort to measure these characteristics, we have obtained the first direct images of the low mass companion to μ Cas A using techniques for high speed correction of image motion at 1.25 and 1.65 μm. These techniques include real-time tracking of the brightest infrared speckle at 75 Hz and of the visible centroid at 500 Hz. Mu Cas B is easily detected with a magnitude difference relative to the primary of >4 at a separation of ~ 1.4 arcsec. Its energy distribution from 0.55 to 3.4 μm yields an effective temperature (3034 ± 160 K), stellar diameter (0.26 $R_\odot$), and luminosity (0.0051 ± 0.0011 $L_\odot$). A direct mass measurement using two photocentric orbits yields 0.15 ± 0.0013 $\mathcal{M}_\odot$. Significant improvements in these parameters can result from astrometric, spectroscopic, and imaging observations of the upcoming periastron passage.

1. INTRODUCTION

The halo binary μ Cas AB (Gliese 53 AB; G5Vp-VI) is known for its potential role in determining the primordial helium abundance. Measurements of the primary star's mass, luminosity, heavy-element abundance, and age can yield the early Galactic helium abundance through stellar evolution theory (Dennis 1965). Of these parameters, the mass has been the most difficult to determine with sufficient accuracy. Since μ Cas AB is an astrometric binary (Wagman 1961; Lippincott 1981; Russell & Gatewood 1984), the component masses can, in principle, be derived from a single measurement of the relative angular separation.

Early attempts to resolve the components of μ Cas AB at visible wavelengths (cf., Wickes 1975) were hindered by the high magnitude difference ($\Delta m_V \sim 6.5$). However, in the near-infrared this difference is significantly less ($\Delta m_K \sim 3.5$), and McCarthy (1984) easily detected the companion at 2.2 and 3.4 μm. More recently, it has also been resolved at 0.85 μm (Karovska *et al.* 1986) and possibly at 1.025 μm (Pierce & Lavery 1985; cf., Sec. IV.a). Despite all these efforts, uncertainty in the photocentric orbit has prevented accurate mass determinations.

Continued imaging at high angular resolution can determine the relative orbit and provide additional photometric information about both stars to help constrain the total and individual masses. Here we present the first direct images of μ Cas AB at 1.25 and 1.65 μm, obtained using two techniques for rapid, real-time compensation of image motion due to atmospheric seeing. These methods, used with modern array detectors, are powerful tools for obtaining sensitive, high angular resolution images in the infrared (Christou 1991).

2. OBSERVATIONS

At infrared wavelengths, the major component of atmospheric seeing is the two-dimensional image motion caused by fluctuations in the slope of the incident wavefront (Fried 1965). In principle, active removal of this component can greatly improve resolution and sensitivity in a long exposure (McCarthy *et al.* 1991). Here we present images of μ Cas AB which demonstrate the performance of these methods in fact.

2.1 Coronagraphy at 1.65 μm by Rapid Centroid Tracking

Images at 1.65 μm were obtained at the Steward Observatory 2.3 m telescope on UT 7 September 1990, with coronagraphic optics (Golimowski *et al.* 1992) coupled to a 58×62 InSb infrared imaging detector (McCarthy *et al.* 1990). The coronagraph features an active mirror for tip/tilt compensation of the wavefront at 500 Hz. The image motion sensor is a CCD quadrant detector receiving visible light from the program object after reflection from either an occulting spot (2.0 arcsec diameter) or a dichroic beamsplitter at the initial focus of the telescope. This focal plane was then reimaged through a pupil plane apodizing mask and focused inside the cold dewar containing the infrared camera.

[1]Observations reported here were obtained at the Multiple Mirror Telescope, a joint facility of the Smithsonian Institution and The University of Arizona.

 0004-6256/93/020652-08$00.90

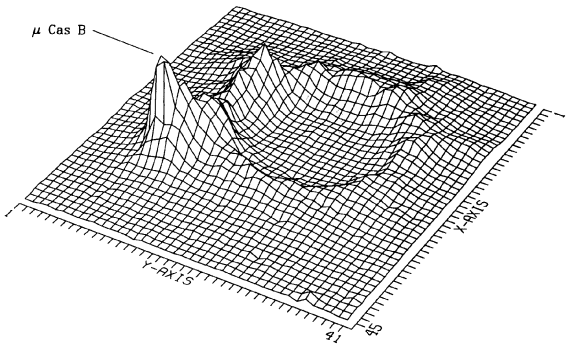

FIG. 1. Coronagraphic image of μ Cas B at 1.65 μm. The occulting spot blocking light from the primary star is 2.0 arcsec in diameter. During the 250 s integration, the visual image of the primary star was actively stabilized by a tip/tilt mirror. The secondary star is seen in the left (NE) corner. The scale is 0.1067 arcsec/pixel.

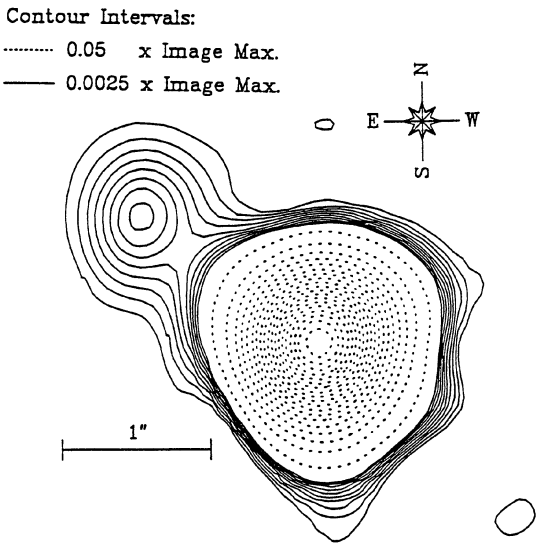

FIG. 2. Deconvolved image of the μ Cas binary system at 1.65 μm. Five hundred one-second short exposures were obtained for both μ Cas and a nearby reference star, SAO 022021, while actively recentering each image's centroid. Shift-and-add post-processing further improved the FWHM of the final image from 0.58 to 0.35 arcsec. The μ Cas image was deconvolved by the reference star image, yielding this diffraction-limited image (FWHM = 0.7 arcsec). The image is normalized to its maximum pixel. The scale is 0.1067 arcsec/pixel (note scale bar).

Our observations of the wide binary α Psc (1.9 arcsec; McAlister & Hartkopf 1988) determined the orientation and pixel scale of the detector, 0.1067 ± 0.0021 arcsec/pixel. The scale corresponds to 0.72 λ/D, which is close to Nyquist sampling of the diffraction limit, λ/D (0.15 arcsec), of the telescope aperture, D. The observing sequence alternated between μ Cas AB and a nearby unresolved source, SAO 022021. Images were obtained with and without both the coronagraphic occulting spot and the active tip/tilt compensation system.

Figure 1 shows a coronagraphic image of μ Cas AB in the standard H band at 1.65 μm. This image was obtained by summing fifty individual 5.0 s exposures while actively correcting for motion of the visual centroid. The faint companion is clearly revealed in the left corner (NE) and can also be seen in a single exposure.

In order to determine the vector separation between both components, we replaced the occulting spot with the dichroic beamsplitter and reobserved μ Cas AB using 500 shorter exposures of 1.0 s each to avoid saturating on the primary star. Although the centroids of these images were actively stabilized by the tip/tilt mirror system, further image sharpening was possible because each short exposure contains a dominant, diffraction-limited speckle whose position fluctuates relative to the centroid due to atmospheric seeing (McCarthy *et al.* 1991). The motion of this speckle can be "tracked" via the technique of shift-and-add (Bates 1982) in postprocessing. Here the individual images were coadded after recentering each on its brightest pixel. The resulting image shows aberrations caused by the coronagraphic optics which were designed for operation at visible wavelengths, not at 1.65 μm. To remove these distortions, we deconvolved the shift-and-add images of μ Cas AB and SAO 022021 by dividing the Fourier transform of the former by that of the latter, then apodized with a Gaussian function with a FWHM of 0.7 arcsec, and performed the inverse transform. Figure 2 shows the final image.

Analysis of the radial profiles of these images shows a continuous improvement in FWHM. The FWHM of the uncorrected image was 0.93 arcsec compared to 0.58 arcsec from centroid tracking and 0.35 arcsec from further processing by the shift-and-add method. The shift-and-add method yields sharper images even though the individual exposure time is relatively long (1.0 s) compared to that normally used to freeze atmospheric seeing ($\sim$0.030 s). Thus, although the speckle structure in the images must be attenuated by the longer exposure, diffraction-limited structure is still present and can be used to advantage.

2.2 Imaging at 1.25 μm by Rapid Speckle Tracking

On UT 23 September 1991, μ Cas AB was imaged in the standard J band at 1.25 μm using a single aperture ("mirror F") of the Multiple Mirror Telescope and the Steward Observatory adaptive optics instrument (Wizinowich *et al.* 1991). For reasons unrelated to this observation, the 1.83 m telescope aperture was baffled down to a diameter of 1.63 m. The instrument utilized only one of its six piezoelectrically controlled subapertures to accomplish tip/tilt control at 75 Hz. The 58×62 InSb camera measured the tip/tilt motion of the image while a HgCdTe camera (NICMOS2; 128×128 pixel) integrated in ten separate 10 s integrations. A beamsplitter was used to illuminate both cameras simultaneously. Both cameras operated in the J photometric band and were also used for identical imaging of the nearby point source SAO 022021.

To achieve image recentering at 75 Hz, a J band image of μ Cas AB was first obtained from a 26×20 subarray of the 58×62 InSb camera through a nondestructive readout in 4.7 ms. At a scale of 0.13 arcsec/pixel, the size of each pixel corresponds to the expected FWHM ($\sim \lambda/D = 0.14$

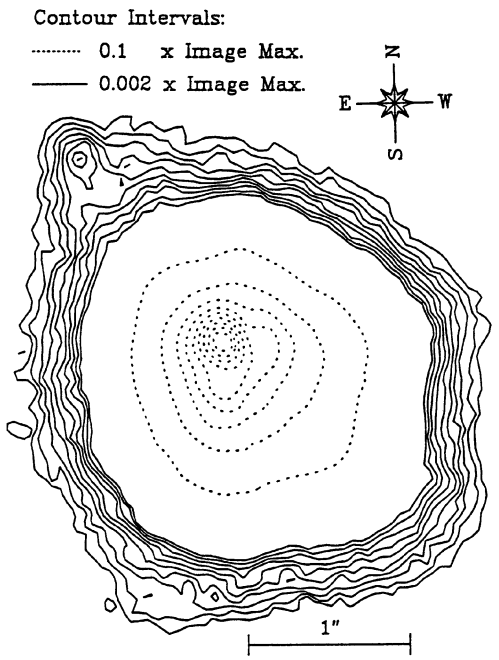

FIG. 3. Image of μ Cas AB at 1.25 μm obtained in a single 50 s exposure with the NICMOS2 camera while tracking at 75 Hz on the brightest speckle of the μ Cas A image using the InSb camera at the same wavelength. The companion is revealed 1.41 arcsec to the NE (upper left) with a magnitude difference of 4.2. The scale is 0.062 arcsec/pixel (note scale bar).

arcsec) of the individual speckles. Second, the location of the brightest speckle, as indicated by the brightest pixel, was determined and the correction voltages sent to the adaptive segment to recenter the image. The full correction loop required 13.2 ms to complete.

Figure 3 shows the full 100 s integration on μ Cas AB from the NICMOS2 camera. The image scale is 0.062 arcsec/pixel. The resolution of this image (FWHM$\sim$0.32 arcsec) falls short of the diffraction-limit (FWHM=0.14 arcsec) and is limited by aberrations in the relay optics ahead of the NICMOS2 camera and possibly also in the telescope. Field rotation due to the altitude/azimuth mount of the MMT contributes only 0.012 arcsec to the image blurring of μ Cas B.

A 20 s integration obtained immediately afterwards on the InSb camera without tip/tilt correction yielded a FWHM of 0.91 arcsec. Since the envelope of the image aberration due to optical surfaces in the telescope and instrument is 0.48 arcsec (Lloyd-Hart 1991), a time-averaged exposure of the shifting image will yield a blur circle of 0.48 arcsec diameter. Assuming the components add in quadrature, we estimate the Fried parameter, r_0, as follows:

$$(0.91)^2=(\lambda/r_0)^2+(0.48)^2.$$

We find $r_0=33$ cm and $D/r_0=4.9$, where $D=1.63$ m is the aperture diameter.

TABLE 1. Observations of μ Cas AB.

Wavelength	1.25 μm	1.65 μm
Epoch	1991.73	1990.69
Separation (arcsec)	1.41±0.051	1.36±0.076
Position angle (deg)	48.6±6.8	48.2±3.1
Magnitude difference	4.2±0.65	4.3±0.25

Under these conditions, light from the faint companion (revealed $\sim$1.4 arcsec to the NE) has been concentrated by a factor of

$$\left(\frac{\text{FWHM uncorrected image}}{\text{FWHM corrected image}}\right)^2 \approx 8,$$

with a resulting improvement in signal to noise.

3. MODEL FITTING

To determine the vector separation and magnitude difference between the components of μ Cas AB from the images in Figs. 2 and 3, we have employed nonlinear least-squares algorithms to fit a model binary star to the data in the Fourier plane (Freeman *et al.* 1991, 1992). We represent each component by a delta function of variable intensity and (x,y) position. The Fourier transform of each is then a complex exponential multiplied by the component intensity. The individual positions are represented by the exponential argument. The resulting model thus contains six free parameters.

This binary model is fit to the complex Fourier transform of each image using the Levenberg–Marquardt algorithm (Press *et al.* 1986) in combination with robust regression. The latter has been shown to reduce the effects of systematic measurements errors in the complex Fourier transform (Freeman *et al.* 1992). This method, known as iteratively reweighted least squares, iteratively assigns weights to the Fourier points based on their agreement with a preliminary fit to the data. In this way, gross errors can be ignored or strongly downweighted.

With this method, the binary model has been fit to the data with results as summarized in Table 1. The fitting region in Fourier space extends from the origin to radii of 3.8 and 1.1 cycles/arcsec for the J and H bands, respectively.

4. DISCUSSION

4.1 The Relative Orbit

Figure 4 illustrates the apparent orbit of μ Cas B relative to μ Cas A, in dashed and dotted curves (Lippincott 1981; Russell & Gatewood 1984) scaled by factors of 4.85 and 5.40, respectively, according to the displayed separation and position angle measurements (cf. section 4.2). The displayed data (this work; Karovska 1986; McCarthy 1984; Wickes 1975; Wickes & Dicke 1974) are those points most soundly determined and most consistent with the astrometric data. Other measurements (Feibelman 1976;

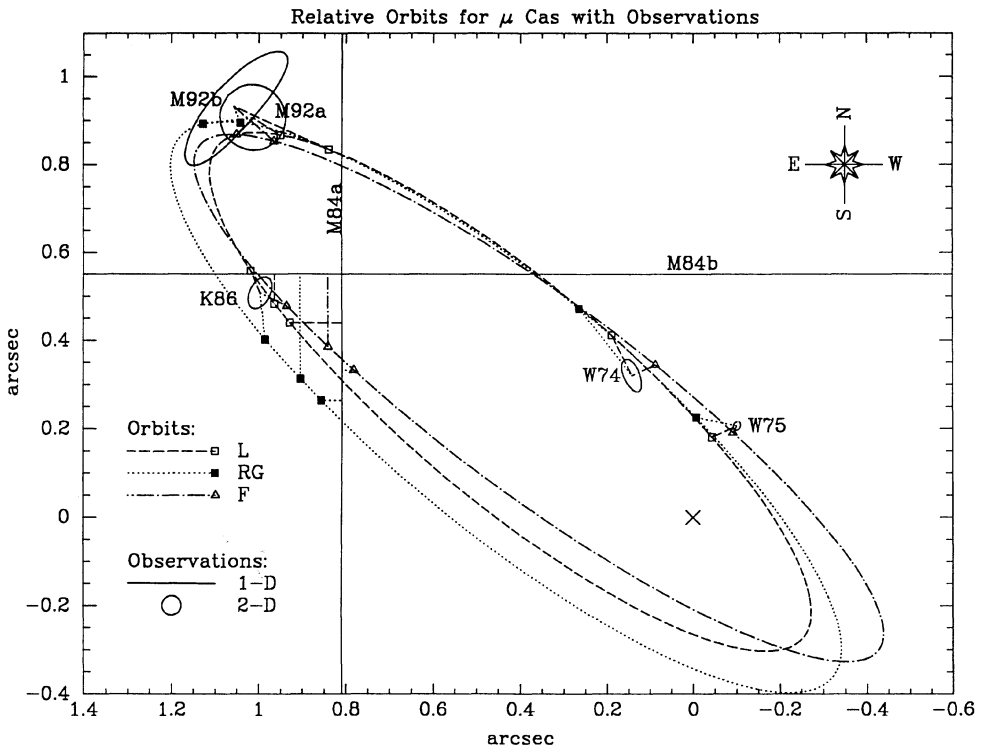

FIG. 4. Observations of μ Cas AB with possible relative orbits labeled as follows: L, from astrometric orbit of Lippincott (1981) with scale factor of 4.85; RG, from Russell & Gatewood (1984) with scale factor of 5.40; *F*, relative orbit fit to two-dimensional observations (see text). Orbit curves are shown in noted line types, with small symbols indicating expected positions from each orbit for each time of observation. Two-dimensional observations are indicated by large ellipses whose axes indicate the size of the 1 σ errors; one-dimensional observations by solid lines. Residuals for one- and two-dimensional observations with respect to each orbit are indicated in the line type of the appropriate orbit. Observations are labeled as in Table 3.

Wehinger & Wyckoff 1966; Hegyi & Curott 1967; Pierce & Lavery 1985) are very inconsistent with the astrometric orbits; some also yield magnitude differences that are now known to be too small.

Although there are only a few two-dimensional measurements of the relative angular separation vector for μ Cas, we have used a nonlinear least-squares method to fit them to a relative orbit based on the observational epoch, period, eccentricity, and Thiele–Innes constants. The separation measurements and their errors are taken directly from this work and from previously published values. The resulting orbital elements are summarized in Table 2 which lists the derived Thiele–Innes constants and their formal errors. This orbit is also included in Fig. 4 (orbit F) for comparison with the astrometric orbits and the available separation measurements. Note that the formal errors in the elements are large due to the small quantity of two-dimensional data currently available.

4.2 Dynamical Mass Measurements

From the separation measurements in Table I, the masses of μ Cas AB can be determined from Kepler's Third Law using the photocentric orbit (cf., McCarthy 1984). The ratio of the observed angular separation to the predicted photocentric separation at the same epoch provides a scale factor, *B*, whose inverse is an excellent approximation to the mass fraction $\mathcal{M}_B/\Sigma\mathcal{M}$. Table 3 summarizes the scale factors measured at the different epochs and wavelengths for each of the two photocentric orbits.

TABLE 2. Relative orbit fit to two-dimensional separation data.

Thiele–Innes constants	*A*(*)	*B*(*)	*F*(*)	*G*(*)
	−0.622±0.11	−0.816±0.12	−0.149±0.28	−0.243±0.27
Dynamical elements	P (yrs)	T_0 (yrs)	e	
	23.5±1.9	1977.62±1.7	0.46±0.13	
Standard orbital elements	a(″)	Ω(°)	ω(°)	i(°)
	0.970	54.3	186.1	104.8

TABLE 3. Observations of μ CaS AB.

Epoch	$\lambda(\mu m)$	Δm	Scale factor	$\lvert\Delta\theta\rvert$ (deg)	Reference
1973.79	0.55	5.5±0.7	3.5±0.93(RG)	5.2± 9.4(RG)	W74
1974.65	0.75	4.5±1.0	5.5±2.9 (RG)	24.5±39.7(RG)	W75
1983.01	2.2	3.5±0.1	5.7±0.44(RG)	17.1± 5.7(RG)	M84a,b
1984.13	0.85	4.9±0.2	5.7±0.4 (RG)	5 ± 6 (RG)	K86
			4.7±0.1 (L)	2 ± 3 (L)	
1990.69	1.65	4.3±0.25	5.1±0.29(RG)	7.8± 3.1(RG)	M92a
			5.1±0.29 (L)	4.1± 3.1 (L)	
1991.73	1.25	4.2±0.25	5.5±0.20(RG)	0.7± 6.8(RG)	M92b
			5.8±0.21 (L)	3.1± 6.8 (L)	

Notes to TABLE 3

L: Lippincott (1981).
W74: Wickes (1974).
M84a,b: McCarthy (1984).
M92a,b: This work.
RG: Russell & Gatewood (1984).
W75: Wickes & Dicke (1975).
K86: Karovska *et al.* (1986).

Uncertainties in these scale factors are caused by errors in the photocentric orbit and in the measured separations.

Beginning with McCarthy (1984), previous investigators have favored the photocentric orbit of Russell & Gatewood (1984) because the resulting masses (0.89, 0.19$\mathcal{M}_\odot$) were more consistent with the indicated stellar luminosities. However, at the present epoch, both orbits predict nearly the same photocentric separation and position angle. Because it is not possible to discriminate between the two orbits, we have calculated for each a weighted average of the scale factors in Table 3 to find $\langle B\rangle_{RG}=5.40\pm0.142$ and $\langle B\rangle_L=4.85\pm0.0778$. The large difference between these values suggests that neither orbit is very accurate and indicates that improved astrometric measurements are required to derive the scale factor.

Individual masses can be calculated from each astrometric orbit using Kepler's Third Law and the measured scale factor, parallax, photocentric semi-major axis, and period. We find

$$\Sigma\mathcal{M}=0.87\pm0.13\mathcal{M}_\odot(\mathrm{RG})$$

$$\Sigma\mathcal{M}=0.70\pm0.048\mathcal{M}_\odot(\mathrm{L}),$$

where the final errors are determined by nearly equal contributions from the first three measured parameters. Since B is the inverse of the fractional mass, $\mathcal{M}_B/\Sigma\mathcal{M}$, we find

$$\mathcal{M}_A=0.71\pm0.11\mathcal{M}_\odot(\mathrm{RG}),$$

$$\mathcal{M}_B=0.16\pm0.024\mathcal{M}_\odot(\mathrm{RG})$$

and

$$\mathcal{M}_A=0.55\pm0.038\mathcal{M}_\odot(\mathrm{L}),$$

$$\mathcal{M}_B=0.14\pm0.010\mathcal{M}_\odot(\mathrm{L}).$$

Curiously, these values are very similar to those derived on previous occasions from Lippincott's orbit which has given consistent masses over the last seven years in contrast to the orbit of Russell & Gatewood (1984).

An independent estimate of the total system mass is provided by the relative orbit itself. Using Kepler's Third Law, a parallax of 0.1368 arcsec (Russell & Gatewood 1984), and the orbital elements from Table 2, we find

$$\Sigma\mathcal{M}=0.65\pm0.85\mathcal{M}_\odot.$$

This mass does not depend on any orbital elements from astrometry but is clearly very uncertain. A factor ~2 improvement in the mass estimate can result from additional separation measurements over the next three years to constrain the relative orbit.

The spectroscopic orbit can also help determine the masses of μ Cas A and μ Cas B and can provide important checks on the orbital parameters derived from astrometry and direct imaging (cf., Marcy & Moore 1989). Using the mass functions from the best available spectroscopic orbit (Duquennoy & Mayor 1991) in combination with the inclinations and scale factors from the astrometric orbits, we find

$$\mathcal{M}_A=1.17\pm0.23\mathcal{M}_\odot(\mathrm{RG}),$$

$$\mathcal{M}_B=0.265\pm0.052\mathcal{M}_\odot(\mathrm{RG})$$

and

$$\mathcal{M}_A=0.843\pm0.17\mathcal{M}_\odot(\mathrm{L}),$$

$$\mathcal{M}_B=0.219\pm0.043\mathcal{M}_\odot(\mathrm{L}).$$

Unfortunately, these errors are two to three times greater than those from astrometry alone. The disagreement (~1–2 σ) may indicate underestimated errors in either method or an inaccurate parallax. However, the accuracy of modern high resolution spectroscopy (Campbell *et al.* 1988; Cochran *et al.* 1991; Marcy & Butler 1991) is much better (±10 to ±50 m/s) and can yield mass estimates comparable to those from astrometry. Figure 5 shows that new measurements obtained around periastron (1994–1998) can distinguish between the two competing astrometric orbits which differ in their radial velocity predictions by 500–2000 m/s.

More precise mass estimates necessitate improved accuracy in all the observational techniques employed here: astrometry, spectroscopy, and direct imaging. By incorporating modern instrumentation and methods, it seems technically feasible to obtain at least a factor two improvement in the uncertainties of the dynamical masses.

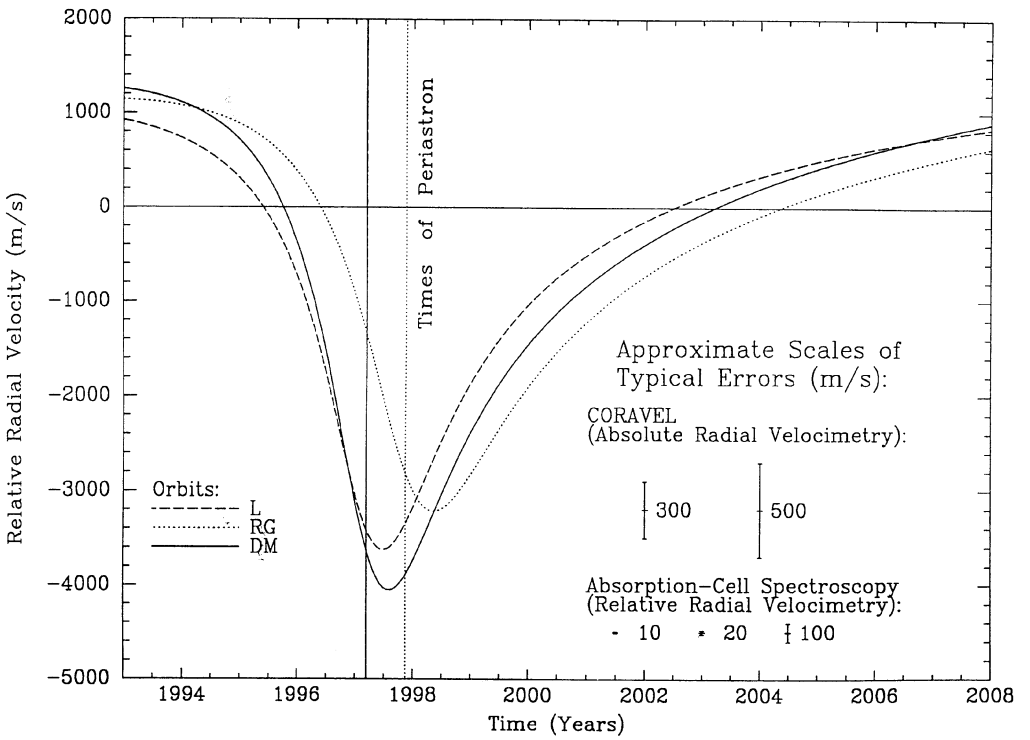

FIG. 5. Possible spectroscopic orbits for μ Cas A, based on astrometric orbits and parallaxes by Lippincott (L; 1981) and Russell & Gatewood (RG; 1984) vs the best measured spectroscopic orbit (DM; Duquennoy & Mayor 1991). The orbit of Duquennoy and Mayor is based on CORAVEL observations from 1977 to 1989, with errors typically from 300–500 m/s. Modern absorption cell radial velocimetry is far more precise, ranging from 5 to 100 m/s (Campbell *et al.* 1988; Cochran *et al.* 1991; Marcy & Butler 1991) but has not yet been applied to this system. Note errorbars shown for comparison.

4.3 Helium Abundance from Measurements of μ Cas B

Dennis (1965) originally showed that the primordial helium abundance could be determined via stellar-interior theory using observational measurements of μ Cas A, specifically its mass, luminosity, age, and heavy element abundance. However, the mass errors remain large due to uncertainties in the photocentric orbit. Also, as discussed by Karovska *et al.* (1986) and Proffitt & Michaud (1991), the primary star may have evolved off the zero age main sequence making this determination more difficult. Since the lower mass secondary, μ Cas B, is most likely still on the main sequence, it offers a better opportunity to determine the helium abundance.

For the first time, the new brightness measurements of μ Cas B in the J and H bands together with existing results at V, R, K, and L constrain its spectral energy distribution and offer a determination of its effective temperature and luminosity. Table 3 lists the measured magnitude differences versus wavelength for μ Cas AB.

In order to determine an effective temperature for μ Cas B, we fit a blackbody distribution to the measured fluxes, F_λ, as shown in Fig. 6, using the relation

$$F_\lambda = \pi\alpha^2 B_\lambda(T),$$

where α is the angular radius of μ Cas B and $B_\lambda(T)$ is the Planck function at temperature T. At 0.85 μm, we have combined the measured magnitude difference obtained in a narrow band by Karovska *et al.* (1986) with a previous I band magnitude (Carney & Aaronson 1979) to obtain photometry at 0.90 μm.

A weighted least-squares fit to all photometric data in Table 3 yields an effective temperature at 3034 ± 160 K and, with a parallax of 0.1368 ± 0.0033 arcsec (Russell & Gatewood 1984), a radius of 0.26 ± 0.0063 $R_\odot$. (Fitting only the *JHKL* infrared data yields 3054 ± 392 K with the same radius.) The resulting luminosity is 0.0051 ± 0.0011 $L_\odot$. For the observed metal abundance of μ Cas A ($Z=0.005$) these values are consistent with a mass of ~ 0.15 $\mathcal{M}_\odot$ (VandenBerg *et al.* 1983) but are not accurate enough to specify a unique mass or helium abundance.

For comparison, the radius–mass relation for eclipsing binaries yields 0.19 $\mathcal{M}_\odot$ after allowing for suspected systematic errors (Lacy 1977). A recent recalibration of the empirical $\mathcal{M}_K$–mass relationship in the solar neighborhood (Henry 1991) yields 0.21 ± 0.021 $\mathcal{M}_\odot$ but does not allow for effects of low metal abundance.

5. CONCLUSIONS

Rapid correction for image motion caused by atmospheric turbulence has yielded the first direct images of μ Cas B and the first direct estimates of its temperature and

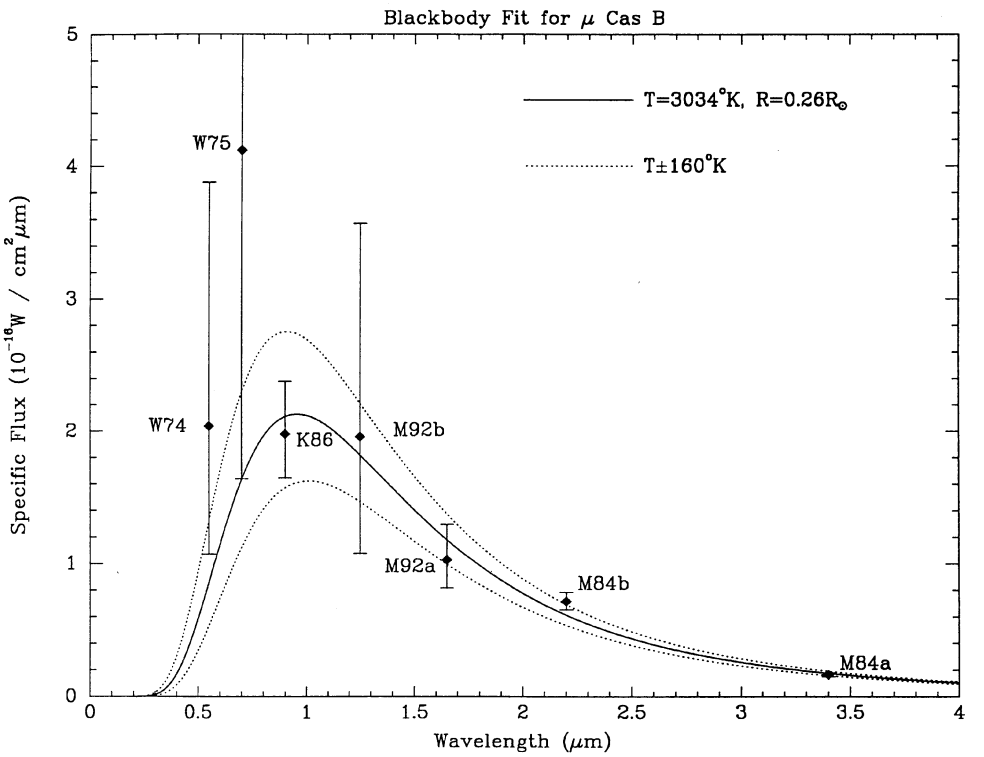

FIG. 6. Photometric measurements of μ Cas vs wavelength. Solid curve results from the best fitting Planck function and stellar radius. Dotted curves show the effect of a one standard deviation range in effective temperature.

luminosity. Analyses of these near-infrared images continue to show that both existing photocentric orbits require revision in order to derive more accurate masses.

Since the companion is now approaching periastron (1997.2–1997.9), new measurements of the relative separations and position angles using the techniques demonstrated in this paper along with new photocentric deviations and position angles and high resolution spectroscopic radial velocities can all be used to improve the accuracy of the orbit, yielding better mass measurements.

Furthermore, although the orbit of μ Cas AB is difficult to determine by any one of these means, all three techniques together can now yield much improved information about it. This is valuable not only for the astrophysical data that an accurate mass can provide but also as a proving ground for testing results from the various techniques. Since each orbital element is measured by at least two of these methods, any observational inconsistencies can be used to characterize the observing techniques.

The authors acknowledge assistance from D. Wittman and R. Dekany in observations at the MMT. The adaptive mirror used at the MMT was provided by ThermoTrex Corp. This project has been supported by NSF Grant No. AST-8822465 (University of Arizona) and by a grant from the Seaver Institution (Johns Hopkins University). B. M. acknowledges support from a National Science Foundation Graduate Research Fellowship.

REFERENCES

Bates, R. H. T. 1982, Physics Reports, 90 203
Campbell, B., Walker, G. A. H., & Yang, S. 1988, ApJ, 331, 902
Carney, B. W., & Aaronson, M. 1979, AJ, 84, 867
Christou, J. C. 1991, PASP, 103, 1040
Cochran, W. D., Hatzes, A. P., & Hancock, T. J. 1991, ApJ, 380, L35
Dennis, T. R. 1965, PASP, 77, 283
Duquennoy, A., & Mayor, M. 1991, A & A, 248, 485
Feibelman, W. A. 1976, ApJ, 209, 497
Freeman, J., Henry, T., & McCarthy, D. 1991, in Proceedings of the ESO Conference on High-Resolution Imaging by Interferometry—II, edited by F. Merkle (European Southern Observatory, Garching) (in press)
Freeman, J., Henry, T., & McCarthy, D. 1992, JOSA (in press)
Fried, D. L. 1965, JOSA, 55, 1427
Golimowski, D. A., Clampin, M., Durrance, S. T., & Barkhouser, R. H. 1992, Appl. Opt., 31, 4405
Hegyi, D. J., & Curott, D. 1970, Phys. Rev. Lett. 24, 415
Henry, T. J. 1991, Ph.D. thesis, University of Arizona
Karovska, M., Nisenson, P., & Stachnik, R. V. 1986, AJ, 92, 898
Lacy, C. 1977, ApJS, 34, 479
Lippincott, S. L. 1981, ApJ, 248, 1053
Lloyd-Hart, M. 1991, Ph.D. thesis, University of Arizona
Marcy, G. W., & Butler, R. P. 1992, PASP (in press)
Marcy, G. W., and Moore, D. 1989, ApJ, 341, 961
McAlister, H. A., & Hartkopf, W. I. 1988, Second Catalog of Interferometric Measurements of Binary Stars, Center for High Angular Resolution Astronomy, Contribution No. 2

McCarthy, D. W. 1984, AJ, 89, 433
McCarthy, D. W., McLeod, B. A., & Barlow, D. 1990, Proc. SPIE, 1237, 496
McCarthy, D. W., McLeod, B. A., Wizinowich, P. L., Freeman, J. D, & Christou, J. C. 1991, unpublished
Pierce, M. J., & Lavery, R. J. 1985, AJ, 90, 647
Press, W. H., Flannery, B. P., Teukolsky, S. A., & Vetterling, W. T. 1986, Numerical Recipes (Cambridge University Press, Cambridge), pp. 521–528
Proffitt, C. R., & Michaud, G. 1991, ApJ, 371, 584
Russell, J. L., & Gatewood, G. 1984, PASP, 96, 429
VandenBerg, D. A., Hartwick, F. D. A., Dawson, P., & Alexander, D. R. 1983, ApJ, 266, 747
Wagman, N. E. 1961, AJ, 66, 433
Wehinger, P. A., & Wyckoff, S. 1966, AJ, 71, 185
Wickes, W. C. 1975, AJ, 80, 655
Wickes, W. C., & Dicke, R. H. 1974, AJ, 79, 1433
Wizinowich, P., *et al.* 1991, Proc. SPIE, 1542, 148
Worek, T. F., & Beardsley, W. R. 1977, ApJ, 217, 134